



Modeling of Fuel Sloshing and its Physical Effects on Flutter

Charbel Farhat,* Edmond Kwan-yu Chiu,† and David Amsallem‡
Stanford University, Stanford, California 94305-4035

Jean-Sébastien Schotté§

Onera, the French Aerospace Laboratory, 92322 Chatillon, France
and

Roger Ohayon¶

Conservatoire National des Arts et Métiers, 75141 Paris, France

DOI: 10.2514/1.J052299

The sloshing effects of an internal fluid on the flutter envelope of an aeroelastic system have received little attention in the open literature. This issue is nevertheless relevant for many aircraft, especially high-performance fighter jets carrying stores. This paper addresses some aspects of this problem as well as related modeling and analysis issues. These include the importance or insignificance of accounting for the hydroelastic effect when modeling an internal fluid and its container as well as accounting for that container when modeling the aerodynamics of the overall aeroelastic system. The paper also reports on the findings of four independent sets of flutter analyses performed for a wing–store test configuration and various fuel fill levels in the subsonic, transonic, and early supersonic regimes. Two of these sets of numerical experiments relied on a computational-fluid-dynamics-based computational technology, and two of them on the doublet-lattice method or a supersonic lifting-surface theory, where applicable. The geometry of the chosen test configuration is that of the AGARD Wing 445.6 with a blunt-nosed store. The obtained computational results show that, at least for the considered wing–store configuration, ignoring the aforementioned hydroelastic effect tends to overestimate the added-mass effect and underestimate the critical pressure and flutter speed. They also reveal that, whereas the aerodynamics of the store may be neglected in the subsonic regime, they cannot be ignored in supersonic air streams. Finally, the performed computational study suggests that, in general, the critical pressure and flutter speed decrease with an increasing fuel fill level.

Nomenclature

A	=	matrix of cell volumes of the fluid grid
b	=	body forces acting on the structure
b_s	=	semichord of the wing at its root
C	=	Jacobian matrix of the numerical flux function with respect to the fluid grid velocity
<i>c</i>	=	arc center
D	=	structural damping matrix
<i>d</i>	=	distance
det	=	determinant of a matrix
div	=	divergence operator
<i>E</i>	=	Young's modulus
E	=	matrix resulting from the time derivative of the product of the fluid cells volumes and the discrete fluid state vector
\tilde{E}	=	fictitious elasticity properties
<i>F</i>	=	external force field acting on the structure
F	=	numerical convective flux function vector

\mathcal{F}	=	fluid convective flux
\mathbf{f}^{ae}	=	vector of external aerodynamic forces acting on the structure
\mathbf{f}^{int}	=	vector of internal forces acting on the structure
\mathbf{f}_m	=	generalized force vector
FSI	=	flutter speed index
G	=	Jacobian matrix of the numerical flux function with respect to the fluid grid position
H	=	Jacobian matrix of the numerical flux function with respect to the discrete fluid state vector
I	=	identity matrix
<i>i</i>	=	pure imaginary number
<i>J</i>	=	Jacobian of a frame transformation
K	=	structural stiffness matrix
$\tilde{\mathbf{K}}'$	=	modified structural stiffness matrix
$\tilde{\mathbf{K}}$	=	pseudostiffness matrix
$\tilde{\mathbf{K}}_c$	=	matrix related to the pseudostiffness matrix
$\tilde{\mathbf{K}}_c$	=	matrix accounting for the effect of the structural motion on the fluid grid at the fluid–structure interface
$\tilde{\mathbf{K}}_F$	=	transmission matrix between the structural displacement vector and the fluid grid position vector
<i>k</i>	=	dimensionless reduced frequency
<i>L</i>	=	length
L_o	=	reference length
\mathbf{M}_A	=	added-mass matrix
\mathbf{M}_F	=	mass matrix of the internal fluid
\mathbf{M}_S	=	structural mass matrix
M_∞	=	freestream Mach number
m_{store}^{empty}	=	mass of an empty store
m_S	=	structural mass of the wing
n_F	=	normal to the fluid–structure interface
n_m	=	number of natural eigenmodes
n_S	=	normal to the surface of the structure
P	=	Jacobian matrix of the vector of external aerodynamic forces with respect to the discrete fluid state vector

Received 24 August 2012; revision received 9 January 2013; accepted for publication 4 March 2013; published online 27 June 2013. Copyright © 2013 by Charbel Farhat. Published by the American Institute of Aeronautics and Astronautics, Inc., with permission. Copies of this paper may be made for personal or internal use, on condition that the copier pay the \$10.00 per-copy fee to the Copyright Clearance Center, Inc., 222 Rosewood Drive, Danvers, MA 01923; include the code 1533-385X/13 and \$10.00 in correspondence with the CCC.

*Department of Aeronautics and Astronautics, Department of Mechanical Engineering, Institute for Computational and Mathematical Engineering, Durand Building, Room 257, 496 Lomita Mall. AIAA Fellow.

†Department of Aeronautics and Astronautics, Durand Building, 496 Lomita Mall. Member AIAA.

‡Department of Aeronautics and Astronautics, Durand Building, Room 028A, 496 Lomita Mall. Member AIAA.

§Department of Aeroelasticity and Structural Dynamics, 29 Avenue de la Division Leclerc. Member AIAA.

¶Structural Mechanics and Coupled System Laboratory, 292 Rue Saint Martin. Fellow AIAA.

\mathbf{P}_m	=	generalized Jacobian matrix of the vector of external aerodynamic forces with respect to the discrete fluid state vector
p	=	pressure fluctuation of the internal fluid
\mathbf{Q}_m	=	generalized aerodynamic force matrix
R	=	radius
r	=	radius
s	=	arc
\mathbf{T}	=	transmission conditions matrix
t	=	time
t_{wall}	=	store wall thickness
\mathbf{u}	=	structural displacement vector
u_F	=	displacement field of the internal fluid
\mathbf{u}_m	=	generalized modal displacement vector
u_S	=	structural displacement field
\mathbf{V}	=	matrix of structural eigenmodes
\hat{V}	=	volume of a conical frustum
V_∞	=	freestream velocity
v_F	=	velocity field of the internal fluid
w	=	fluid state vector
\mathbf{w}	=	discrete fluid state vector
x	=	position vector field
\mathbf{x}	=	fluid grid position vector
x_F	=	displacement field of a fluid grid point
Γ	=	fluid free surface
$\delta(\cdot)$	=	perturbation of a quantity
$\partial\Omega_S$	=	surface of the structure
$\tilde{\epsilon}$	=	fictitious strain tensor
ϵ_S	=	strain tensor
λ	=	square of the circular frequency
$\bar{\mu}$	=	ratio of the structural mass of the empty store and the product of the freestream density and the frustum volume
ν	=	Poisson's ratio
ξ	=	reference position of a fluid grid point
π	=	pressure constant
$\tilde{\rho}$	=	fictitious density
$\rho_{\text{aluminium}}$	=	aluminium density
ρ_F	=	density of the internal fluid
ρ_S	=	structural density
ρ_∞	=	freestream density
Σ	=	fluid–structure interface boundary
σ_S	=	structural stress tensor
τ	=	dimensionless time
Φ	=	vector of fluid potential degrees of freedom
ϕ	=	potential function for the internal fluid
ψ	=	angle
ω	=	(circular) frequency
Ω	=	diagonal matrix containing the circular frequencies of the structure
Ω_F	=	internal fluid domain
Ω_S	=	structural domain
ω_α	=	first dry torsional mode frequency of the structure
∇	=	gradient operator
Δ	=	Laplace operator
$-$	=	dimensionless quantity
\cdot	=	dimensionless time derivative

Subscripts

a	=	amplitude
cyl	=	store cylinder quantity
LE	=	store leading-edge quantity
o	=	equilibrium configuration
t	=	time derivative
*	=	quantity satisfying the free surface Dirichlet boundary conditions

Superscripts

cr	=	critical value
----	---	----------------

I	=	imaginary part
R	=	real part

I. Introduction

THE numerous effects of an internal fluid on the overall behavior of an aircraft or spacecraft have long been recognized by the aircraft design community [1,2]. In particular, criteria for designing launch vehicles to accommodate the sloshing effect of an internal propellant [3] have been documented. Unfortunately, whether derived from experimental or computational data [3,4], these criteria did not in general incorporate the flexibility effect of the fluid container. For this reason, these criteria do not address the flutter issue, which is often finally resolved by a flutter flight test.

The cost of a flutter flight test campaign increases rapidly with the number of configurations requiring certification [5,6]. In the presence of stores containing an internal fluid, the fill level becomes an additional configuration parameter. Perhaps because of the already large number of other parameters to consider and the already substantial cost associated with flight testing, it seems that there is very little, if any, focus on the effects of the interaction between an internal fluid and its containing structure during flutter flight tests.

There have been, however, some experimental attempts to investigate the effects of an internal fluid on flutter. In particular, it was observed in [7] that the dynamic response of a coupled fluid–tank system can exhibit modal resonances that are not predicted by any uncoupled analysis. It was also reported in [8] that the presence of fuel between wing panels can alter their flutter characteristics. Little computational research has been performed, however, for predicting the effects of the presence of an internal fluid on flutter [9,10].

Therefore, the main objective of the work reported here is to numerically predict the effects on flutter of the interaction between an internal fluid and its containing flexible structure. To this effect, two different representations of the internal fluid are considered. The first one aims at capturing accurately the hydroelastic vibrations of such a fluid and its store. The second one aims instead at reducing model preparation time and leads to considering other assumptions such as, for example, ignoring the aerodynamics of the store. In all cases, different computational technologies are considered for representing the external fluid. These are the versatile linearized computational fluid dynamics (CFD) approach, and the doublet-lattice method and a lifting-surface theory, which remain popular for compressible subsonic flows and supersonic ones, respectively, particularly in the design environment. Consequently, a secondary objective of this work is to report on the impact of these modeling issues on the prediction of the sloshing effects on flutter.

To this effect, the remainder of this paper is organized as follows.

In Sec. II, two different computational models are described for representing an internal fluid. In Sec. III, a higher-fidelity computational framework for aeroelasticity based on linearized CFD and lower-fidelity alternatives based on the linear aerodynamic theory are overviewed. In Sec. IV, the results of the flutter analysis of a wing–store geometry based on the AGARD Wing 445.6 and the various modeling approaches outlined previously are reported and discussed for various fuel fill levels. Finally, Sec. V concludes this paper.

Remark: In general, slosh refers to the movement of an internal fluid with a free surface in the presence of gravity [11]. However, such a slosh occurs at frequencies that are too low to be of concern to flutter. Therefore, in this work, the effect of gravity on the movement of the internal fluid is ignored, but for the sake of simplicity, the movement of that fluid is still referred to as slosh.

II. Mathematical Models for an Internal Fluid

Here, two approaches of different fidelity levels are considered for accounting for the effects of an internal fluid in flutter prediction. The first approach is based on the theory of hydroelastic vibrations of an elastic structure containing an inviscid fluid. It results in an added-mass model that captures the hydroelastic effect [11]. The second approach accounts only for the mass and inertia of an internal fluid

and leads to a trivial added-mass model [12]. It minimizes model preparation time. It also leads to considering the possibility of neglecting the aerodynamics of the container, which can be attractive for parametric store-configuration studies. Both of these models can, however, be easily integrated in existing aeroelastic flutter-computation procedures.

A. Hydroelastic Vibrations Model

Here, the flexible store and the fluid it may contain are viewed as a coupled hydroelastic system. The internal fluid occupying a domain Ω_F with a free surface Γ and a fluid–structure interface Σ (see Fig. 1) is assumed to be inviscid, incompressible, homogeneous, weightless, and without surface tension. Hence, its dynamic behavior is governed by the linearized Euler equations

$$\nabla p = -\rho_F \frac{\partial^2 u_F}{\partial t^2} \tag{1}$$

where $p, \rho_F,$ and u_F denote the Eulerian pressure fluctuation, density, and displacement of the fluid, respectively, and t denotes time. Furthermore, assuming that it is characterized by small displacement amplitudes, the fluid motion can be assumed to be harmonic and is therefore represented by

$$u_F = u_{F_a} \cos \omega t \tag{2a}$$

$$p = p_a \cos \omega t \tag{2b}$$

where the subscript a designates the amplitude, and ω denotes the circular frequency. From Eqs. (1), (2a), and (2b), it follows that

$$p = \rho_F \omega^2 \phi + \pi \tag{3}$$

where ϕ is the potential function satisfying $\nabla \phi = u_F,$ and π is an arbitrary constant that is set here to $\pi = 0.$ After some manipulations, the incompressibility condition $\nabla \cdot v_F(x', t) = 0,$ where v_F denotes the fluid velocity and $x' = x + u_F(x, t),$ leads to

$$\Delta \phi = 0 \text{ in } \Omega_F \tag{4}$$

The structural vibrations are also assumed to be harmonic with small amplitudes. Hence, they are represented by the dynamic equations of equilibrium

$$\sigma_{S_{ij}}(u_S) + \rho_S \omega^2 u_{S_i} = 0 \text{ in } \Omega_S \tag{5a}$$

$$\sigma_{S_{ij}}(u_S) n_{S_j} = F_i \text{ on } \partial \Omega_S \setminus \Sigma \tag{5b}$$

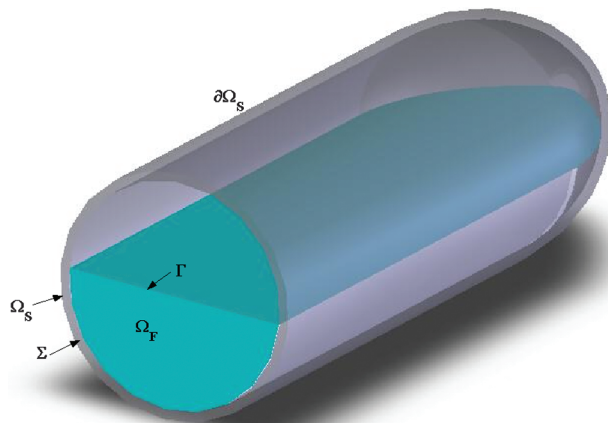


Fig. 1 Cut-away view of a typical store showing the definition of the various domains and interfaces.

where $\sigma_{S_{ij}}$ denotes the stress tensor components ($i = 1, 2, 3,$ $j = 1, 2, 3$) of the structure $\Omega_S;$ ρ_S and u_S denote the density and displacement of the structure, respectively; a comma denotes a partial spatial derivative; the subscripts i and j designate the i th and j th components of a quantity in three dimensions, respectively; n_S denotes the normal to the surface of the structure $\partial \Omega_S;$ and F denotes the prescribed external force field acting on the structure.

The transmission conditions coupling the fluid and structure components of the hydroelastic system at the fluid–structure interface Σ can be written as

$$\sigma_{S_{ij}}(u_S) n_{S_j} = \rho_F \omega^2 \phi n_{F_i} \tag{6}$$

where n_F denotes the normal to the fluid–structure interface Σ from the fluid side, and

$$\frac{\partial \phi}{\partial n_F} = u_S \cdot n_F \tag{7}$$

The first of the previous two equations expresses the conservation of momentum at $\Sigma;$ the second one is equivalent to a nonpenetration condition at this interface.

Finally, on the free surface Γ of the fluid (see Fig. 1), pressure invariance yields the following boundary condition:

$$p = \rho_F g u_{F_3} = 0 \tag{8}$$

(as $\rho_F g = 0$ due to the weightless assumption) where the subscript 3 designates the coordinate in the vertical direction. This yields $\phi = 0$ on the surface; see Eq. (3).

In summary, the boundary-value problem (BVP) governing the vibrations of a system comprising a store and an internal fluid is given by

$$\begin{aligned} \Delta \phi &= 0 \text{ in } \Omega_F \\ \phi &= 0 \text{ on } \Gamma \\ \frac{\partial \phi}{\partial n_F} &= u_S \cdot n_F \text{ on } \Sigma \\ \sigma_{S_{ij}}(u_S) n_{S_j} &= \rho_F \omega^2 \phi n_{F_i} \text{ on } \Sigma \\ \sigma_{S_{ij,j}}(u_S) + \rho_S \omega^2 u_{S_i} &= 0 \text{ in } \Omega_S \\ \sigma_{S_{ij}}(u_S) n_{S_j} &= F_i \text{ on } \partial \Omega_S \setminus \Sigma \end{aligned}$$

and the pressure p of the internal fluid is obtained from Eq. (3). Note that, with the choice $\pi = 0,$ the previous BVP remains well-posed [11] for $\omega = 0.$

The finite-element discretization of the previous BVP leads to the following system of matrix equations:

$$\begin{bmatrix} \mathbf{K} - \lambda \mathbf{M}_S & -\lambda \mathbf{T}_* \\ -\mathbf{T}_*^T & \mathbf{M}_{F_*} \end{bmatrix} \begin{bmatrix} \mathbf{u} \\ \Phi_* \end{bmatrix} = \mathbf{0} \tag{9}$$

where $\lambda = \omega^2,$ $\mathbf{K},$ and \mathbf{M}_S denote the standard structural stiffness and mass matrices; \mathbf{M}_{F_*} is the standard internal fluid mass matrix; \mathbf{T} is the matrix arising from the finite-element discretization of the transmission conditions [Eqs. (6) and (7)]; \mathbf{u} and Φ_* denote the vectors of structural displacements and fluid potential degrees of freedom, respectively; the $*$ subscript specifies that the finite-element space in which ϕ is approximated satisfies the Dirichlet boundary condition $\phi = 0$ on $\Gamma;$ and the superscript T designates the transpose operation. Because \mathbf{M}_{F_*} is nonsingular, the second row of the previous matrix equation gives

$$\Phi_* = \mathbf{M}_{F_*}^{-1} \mathbf{T}_*^T \mathbf{u} \tag{10}$$

which transforms the system of Eq. (9) into the following simpler equation:

$$\mathbf{K}\mathbf{u} - \lambda(\mathbf{M}_S + \mathbf{M}_A)\mathbf{u} = \mathbf{0} \quad (11)$$

where

$$\mathbf{M}_A = \mathbf{T}_* \mathbf{M}_{F_*}^{-1} \mathbf{T}_*^T \quad (12)$$

is the ‘‘added-mass’’ finite-element matrix. In the remainder of this paper, Eq. (11) is referred to as the consistent or hydroelastic added-mass model of the flutter problem in the presence of an internal fluid.

B. Frozen-Mass Model

A trivial approximation of the added-mass effect of an internal fluid is obtained by lumping at one or more points the mass and inertia of this fluid. Compared to the previous modeling approach, this simpler one reduces model preparation time because it eliminates the need to create a new mesh for the internal fluid for every fill level of interest. It also leads to considering the possibility of neglecting the aerodynamics of the store in the flutter analysis. The latter assumption enables the application of popular supersonic lifting-surface theories that nevertheless lack the capability of handling slender bodies to modeling the unsteady external aerodynamics of the given aeroelastic system; for example, see Sec. III.B.2. More importantly, this further assumption simplifies the flutter analysis of parametric store configurations and therefore the modeling and simulation of store clearance, and it significantly reduces the associated model preparation time.

For convenience, the previous approach is implemented in this work by treating the fluid as an almost-incompressible medium with the same total mass and density (and hence volume) as the original body of fluid. The shape and location of this medium are chosen to be those assumed by the internal fluid when the store is completely horizontal and at rest. The Poisson ratio of this medium is chosen to be close enough to the incompressible limit of 0.5, while still preventing finite-element locking during any phase of the numerical analysis. Its elastic modulus is chosen to be significantly lower than that of the containing structure.

III. Computational Frameworks for Flutter Analysis

Two well-proven computational frameworks of different level of fidelity are also considered for analyzing the effect of fuel sloshing on flutter. The first one is a higher-fidelity framework because it is based on the Euler equations for modeling the external flow and the linearized three-field arbitrary Lagrangian–Eulerian (ALE) [13–16] formulation of fluid–structure interaction for modeling aeroelastic effects. The second computational framework is a lower-fidelity but more computationally economical one. In the subsonic domain, it is based on the standard doublet-lattice method (DLM), which uses the linearized aerodynamic potential theory [17,18] to predict the aerodynamic loads on lifting surfaces and slender bodies. In the supersonic regime, it is based on a similar linear theory [19] that is, however, limited to planar lifting surfaces and therefore cannot handle stores. This theory and associated software are most convenient for studying here the effect of neglecting the aerodynamics of a store on an overall flutter analysis. The higher-fidelity computational framework is reviewed in more detail than the lower-fidelity one because it is not as popular yet.

In both computational frameworks, finite-element modal reduction is used for representing a structure.

A. Linearized Computational-Fluid-Dynamics-Based Computational Framework

This framework is considered here for four main reasons.

1) It is based on a perturbation theory, and flutter is essentially a perturbation problem.

2) Unlike linear methods, it incorporates the effects of shocks in the transonic regime and is valid in all of the subsonic, transonic, and supersonic regimes.

3) Unlike nonlinear methods, it is fast enough to appeal to production environments.

4) It is compatible with the added-mass model of the internal fluid presented in Sec. II.A because the hydroelastic model itself is also a linearized model based on a perturbation theory [11].

1. Three-Field Formulation of Aeroelastic Problems

The three-field formulation of nonlinear computational aeroelasticity introduced more than a decade ago [20] models a fluid–structure interaction problem by three coupled partial differential equations: one governing the fluid subsystem and written in an ALE coordinate system to facilitate the treatment of moving boundary surfaces, one governing the motion of the fluid mesh induced by the motion of boundary surfaces, and one governing the dynamic equilibrium of the structural subsystem driving the motion of these boundary surfaces. In the case of inviscid flows, these three equations can be written as

$$\frac{\partial Jw}{\partial t} \Big|_{\xi} + J\nabla_x \cdot \left(\mathcal{F}(w) - \frac{\partial x_F}{\partial t} w \right) = 0 \quad (13a)$$

$$\rho_S \frac{\partial^2 u_S}{\partial t^2} - \text{div}(\sigma_S(\epsilon_S(u_S))) = b \quad (13b)$$

$$\tilde{\rho} \frac{\partial^2 x_F}{\partial t^2} - \text{div}(\tilde{E} : \tilde{\epsilon}(x_F)) = 0 \quad (13c)$$

where ξ and $x_F(t)$ denote the reference position of a fluid grid point and the time-dependent displacement of a fluid grid point, respectively; $J = \det(dx_F/d\xi)$ is the Jacobian of the frame transformation $\xi \rightarrow x_F$; \mathcal{F} denotes the convective flux associated with the fluid state vector w ; ϵ_S is the strain tensor of the structure; b denotes the body forces acting on the structure; and $\tilde{\rho}$, \tilde{E} , and $\tilde{\epsilon}$ denote the fictitious density, elasticity properties, and strain tensor of the pseudostructural system adopted for modeling the moving fluid grid, respectively. All other variables have the same meaning as before.

The finite volume (fluid) and finite-element (structure) semi-discretizations of the previous equations lead to

$$(\mathbf{A}(\mathbf{x}_F)\mathbf{w})_{,t} + \mathbf{F}(\mathbf{w}, \mathbf{x}_F, \mathbf{x}_{F,t}) = \mathbf{0} \quad (14a)$$

$$\mathbf{M}_S \mathbf{u}_{,tt} + \mathbf{f}^{\text{int}}(\mathbf{u}, \mathbf{u}_{,t}) - \mathbf{f}^{\text{ae}}(\mathbf{u}, \mathbf{w}) = \mathbf{0} \quad (14b)$$

$$\tilde{\mathbf{K}} \mathbf{x}_F - \tilde{\mathbf{K}}_c \mathbf{u} = \mathbf{0} \quad (14c)$$

where \mathbf{A} denotes the diagonal matrix of cell volumes; \mathbf{w} and \mathbf{x} denote the fluid state and fluid grid position semidiscrete vectors, respectively; a subscript $,t$ designates a time derivative; \mathbf{F} denotes the vector of numerical convective flux functions; \mathbf{M}_S is the finite-element mass matrix of the structure; \mathbf{u} is the semidiscrete displacement vector; \mathbf{f}^{int} and \mathbf{f}^{ae} denote the vectors of internal and external aerodynamic forces acting on the structure, respectively; $\tilde{\mathbf{K}}$ and $\tilde{\mathbf{K}}_c$ are pseudostiffness matrices; and $\tilde{\mathbf{K}}_c$ accounts for the effect of the structural motion on the fluid mesh at the interface between the structure and the external fluid [21].

2. Linearization Around an Equilibrium Configuration

Consider an aeroelastic system in an equilibrium configuration ($\mathbf{w}_o, \mathbf{w}_{,t_o} = \mathbf{0}, \mathbf{x}_{F_o}, \mathbf{x}_{F,t_o} = \mathbf{0}, \mathbf{u}_o, \mathbf{u}_{,t_o} = \mathbf{0}, \mathbf{u}_{,tt_o} = \mathbf{0}$) designated by the subscript o . To rapidly compute the response of this system to a perturbation of the form $(\delta\mathbf{w}, \delta\mathbf{w}_{,t}, \delta\mathbf{x}_F, \delta\mathbf{x}_{F,t}, \delta\mathbf{u}, \delta\mathbf{u}_{,t}, \delta\mathbf{u}_{,tt})$, which can be used to identify the aeroelastic parameters of this system and determine its stability or flutter, the problem unknowns are expanded as follows:

$$\mathbf{w} = \mathbf{w}_o + \delta\mathbf{w}, \quad \mathbf{w}_{,t} = \delta\mathbf{w}_{,t}, \quad \mathbf{x}_F = \mathbf{x}_{F_o} + \delta\mathbf{x}_F, \quad \mathbf{x}_{F,t} = \delta\mathbf{x}_{F,t} \quad (15)$$

$$\mathbf{u} = \mathbf{u}_o + \delta\mathbf{u}, \quad \mathbf{u}_{,t} = \delta\mathbf{u}_{,t}, \quad \mathbf{u}_{,tt} = \delta\mathbf{u}_{,tt} \quad (16)$$

and Eqs. (14a–14c) are linearized as follows.

First, the fluid equations are linearized around the equilibrium configuration and rewritten in dimensionless form following the approach first described in [13,14]. This transforms Eq. (14a) into

$$\bar{\mathbf{A}}_o \delta \dot{\bar{\mathbf{w}}} + \bar{\mathbf{H}}_o \delta \bar{\mathbf{w}} + (\bar{\mathbf{E}}_o + \bar{\mathbf{C}}_o) \delta \dot{\bar{\mathbf{x}}}_F + \bar{\mathbf{G}}_o \delta \bar{\mathbf{x}}_F = \mathbf{0} \quad (17)$$

where

$$\begin{aligned} \bar{\mathbf{A}}_o &= \bar{\mathbf{A}}(\bar{\mathbf{x}}_{F_o}) & \bar{\mathbf{H}}_o &= \frac{\partial \bar{\mathbf{F}}}{\partial \bar{\mathbf{w}}}(\bar{\mathbf{w}}_o, \bar{\mathbf{x}}_{F_o}) & \bar{\mathbf{E}}_o &= \frac{\partial \bar{\mathbf{A}}}{\partial \bar{\mathbf{x}}_F}(\bar{\mathbf{x}}_{F_o}) \bar{\mathbf{w}}_o \\ \bar{\mathbf{C}}_o &= \frac{\partial \bar{\mathbf{F}}}{\partial \dot{\bar{\mathbf{x}}}_F}(\bar{\mathbf{w}}_o, \bar{\mathbf{x}}_{F_o}) & \bar{\mathbf{G}}_o &= \frac{\partial \bar{\mathbf{F}}}{\partial \bar{\mathbf{x}}_F}(\bar{\mathbf{w}}_o, \bar{\mathbf{x}}_{F_o}) \end{aligned}$$

Here, and throughout the remainder of this section, the bar notation indicates that a quantity is dimensionless, and a dot designates the derivative with respect to the dimensionless time:

$$\tau = \left(\frac{V_\infty}{L_o} \right) t \quad (18)$$

where L_o denotes a reference length, and V_∞ is the freestream velocity.

The matrices $\bar{\mathbf{H}}_o$, $\bar{\mathbf{G}}_o$, and $\bar{\mathbf{C}}_o$ result from a first-order Taylor expansion of the vector of numerical flux functions around the equilibrium configuration $(\bar{\mathbf{w}}_o, \bar{\mathbf{x}}_{F_o})$. The matrix $\bar{\mathbf{H}}_o$ has, in general, a rank equal to the number of fluid degrees of freedom (DOF). The matrix $\bar{\mathbf{E}}_o$ results from a similar expansion of the time derivative of the product of the cell volumes and the fluid state vector.

Next, the structural subsystem [Eq. (14b)] is linearized around the equilibrium state $(\mathbf{w}_o, \mathbf{x}_{F_o}, \mathbf{u}_o)$ to obtain

$$\mathbf{M}_S \delta \mathbf{u}_{,tt} + \mathbf{D}_o \delta \mathbf{u}_{,t} + \mathbf{K}' \delta \mathbf{u} = \mathbf{P}_o \delta \bar{\mathbf{w}} \quad (19)$$

where

$$\begin{aligned} \mathbf{K}_o &= \frac{\partial \mathbf{f}^{\text{int}}}{\partial \mathbf{u}}(\mathbf{u}_o) & \mathbf{K}' &= \mathbf{K}_o - \frac{\partial \mathbf{f}^{\text{ac}}}{\partial \mathbf{u}}(\mathbf{w}_o, \mathbf{u}_o) \\ \mathbf{D}_o &= \frac{\partial \mathbf{f}^{\text{int}}}{\partial \mathbf{u}_{,t}}(\mathbf{u}_o) & \mathbf{P}_o &= \frac{\partial \mathbf{f}^{\text{ac}}}{\partial \bar{\mathbf{w}}}(\mathbf{w}_o, \mathbf{u}_o) \end{aligned}$$

To keep the notation as compact as possible, the subscript o and the prefix δ are dropped in the remainder of this paper. Hence, the same variables \mathbf{w} , \mathbf{x}_F , and \mathbf{u} are used next to denote the perturbations around the chosen equilibrium configuration of the fluid state, fluid mesh motion, and structural motion vectors, respectively.

Then, the dimensionless fluid mesh position and velocity variables $\bar{\mathbf{x}}$ and $\dot{\bar{\mathbf{x}}}$ are eliminated from the coupled system of linearized equations by introducing

$$\tilde{\mathbf{K}}_F = \tilde{\mathbf{K}}^{-1} \tilde{\mathbf{K}}_c \quad (20)$$

so that

$$\bar{\mathbf{x}}_F = \tilde{\mathbf{K}}_F \bar{\mathbf{u}} \quad \dot{\bar{\mathbf{x}}}_F = \tilde{\mathbf{K}}_F \dot{\bar{\mathbf{u}}} \quad (21)$$

where

$$\bar{\mathbf{u}} = \frac{\mathbf{u}}{L_o} \quad (22)$$

and \mathbf{u} is measured with respect to the equilibrium configuration. The previous algebraic manipulations allow rewriting Eq. (17) as

$$\bar{\mathbf{A}} \dot{\bar{\mathbf{w}}} + \bar{\mathbf{H}} \bar{\mathbf{w}} + (\bar{\mathbf{E}} + \bar{\mathbf{C}}) \tilde{\mathbf{K}}_F \dot{\bar{\mathbf{u}}} + \bar{\mathbf{G}} \tilde{\mathbf{K}}_F \bar{\mathbf{u}} = \mathbf{0} \quad (23)$$

Next, neglecting the effects of $\frac{\partial \mathbf{f}^{\text{ac}}}{\partial \mathbf{u}}|_o$ and \mathbf{D}_o , that is assuming that $\mathbf{K}' \approx \mathbf{K}_o$ and no structural damping, Eq. (19) is projected onto a modal basis \mathbf{V} of n_m dry, natural, structural modes and therefore is transformed into

$$\mathbf{I} \mathbf{u}_{m,tt} + \Omega^2 \mathbf{u}_m = \mathbf{P}_m \bar{\mathbf{w}} \quad (24)$$

Here, \mathbf{I} denotes the identity matrix, Ω^2 is a diagonal matrix containing the squares of n_m natural circular frequencies of the structure, and the subscript m designates generalized modal quantities, e.g., \mathbf{u}_m denotes the generalized modal displacement coordinates and $\mathbf{P}_m \bar{\mathbf{w}}$ the generalized aerodynamic forces satisfying

$$\mathbf{u} = L_o \bar{\mathbf{u}} = \mathbf{V} \mathbf{u}_m \quad \mathbf{P}_m = \mathbf{V}^T \mathbf{P} \quad (25)$$

In summary, Eqs. (23) and (24) constitute the governing linearized equations of motion of an aeroelastic system. They can be solved either in the time or frequency domain to determine the flutter characteristics of this system. Both computational approaches are briefly reviewed next.

3. Flutter Analysis in the Time Domain

To perform the flutter analysis of a given aeroelastic system, a pertinent initial perturbation can be defined, and a numerically stable and provably second-order time-accurate staggered solution procedure [22–24] can be applied to the time integration of the coupled fluid [Eq. (23)] and structural [Eq. (24)] semidiscrete equations of equilibrium. In this case, analyzing the predicted response of the aeroelastic system by a modal identification procedure, for example, an eigenrealization algorithm such as ERA [25], determines the flutter characteristics of the aeroelastic system.

4. Flutter Analysis in the Frequency Domain

Equations (23) and (24) can be transformed into the frequency domain and manipulated to define a generalized aerodynamic force matrix. Then, the flutter analysis of the aeroelastic system of interest can be performed in the frequency domain by substituting this matrix into the frequency domain counterpart of Eq. (24) and applying the $p-k$ method [26,27] to the resulting dynamic equation as described next.

Let

$$k = \left(\frac{L_o}{V_\infty} \right) \omega \quad (26)$$

denote the dimensionless reduced frequency. From this definition and that of the dimensionless time [Eq. (18)], it follows that

$$\omega t = k \tau \quad (27)$$

Let also

$$\mathbf{f}_m^{\text{ac}} = \mathbf{P}_m \bar{\mathbf{w}} \quad (28)$$

denote the generalized aerodynamic forces appearing in Eq. (24). In the frequency domain, $\bar{\mathbf{w}}$, \mathbf{u}_m , and \mathbf{f}_m^{ac} can be expressed as

$$\bar{\mathbf{w}} = \bar{\mathbf{w}}^a e^{ikt} \quad \mathbf{u}_m = \mathbf{u}_m^a e^{ikt} \quad \mathbf{f}_m^{\text{ac}} = \mathbf{f}_m^{\text{ac}a} e^{ikt} \quad (29)$$

where i is the pure imaginary number satisfying $i^2 = -1$; and $\bar{\mathbf{w}}^a$, \mathbf{u}_m^a , and $\mathbf{f}_m^{\text{ac}a}$ denote the amplitudes of $\bar{\mathbf{w}}$, \mathbf{u}_m , and \mathbf{f}_m^{ac} , respectively.

Substituting the first two of Eq. (29) into Eq. (23) and using the first of Eq. (25) leads to

$$\bar{\mathbf{w}}^a(k) = - \left(\frac{1}{L_o} \right) (ik \bar{\mathbf{A}} + \bar{\mathbf{H}})^{-1} (ik(\bar{\mathbf{E}} + \bar{\mathbf{C}}) + \bar{\mathbf{G}}) \tilde{\mathbf{K}}_F \mathbf{V} \mathbf{u}_m^a \quad (30)$$

From Eq. (28), the second of Eq. (25), the third of Eq. (29), and Eq. (30), it follows that

$$\begin{aligned} \mathbf{f}_m^{\text{ac}a}(k) &= \mathbf{V}^T \mathbf{P} \bar{\mathbf{w}}^a(k) = - \left(\frac{1}{L_o} \right) \mathbf{V}^T \mathbf{P} (ik \bar{\mathbf{A}} + \bar{\mathbf{H}})^{-1} \\ &\times (ik(\bar{\mathbf{E}} + \bar{\mathbf{C}}) + \bar{\mathbf{G}}) \tilde{\mathbf{K}}_F \mathbf{V} \mathbf{u}_m^a = \mathbf{Q}_m \mathbf{u}_m^a \end{aligned} \quad (31)$$

where

$$\mathbf{Q}_m(k) = -\left(\frac{1}{L_o}\right) \mathbf{V}^T [\mathbf{P}(ik\bar{\mathbf{A}} + \bar{\mathbf{H}})^{-1}(ik(\bar{\mathbf{E}} + \bar{\mathbf{C}}) + \bar{\mathbf{G}})\bar{\mathbf{K}}_F] \mathbf{V} \quad (32)$$

is the generalized aerodynamic force complex matrix of size n_m equal to the dimension of the structural modal basis.

Now, from definition (18), the second of Eq. (29), the definition of the reduced frequency [Eq. (26)], and Eq. (27), it follows that

$$\mathbf{u}_{m,i} = i\omega \mathbf{u}_m \quad (33)$$

Next, decomposing \mathbf{Q}_m into its real part \mathbf{Q}_m^R and imaginary part \mathbf{Q}_m^I and using the previous identity leads to

$$\mathbf{P}_m \bar{\mathbf{w}} = \mathbf{f}_m^{\text{ac}} = \mathbf{Q}_m \mathbf{u}_m = \mathbf{Q}_m^R \mathbf{u}_m + i\mathbf{Q}_m^I \mathbf{u}_m = \mathbf{Q}_m^R \mathbf{u}_m + \frac{1}{\omega} \mathbf{Q}_m^I \mathbf{u}_{m,i} \quad (34)$$

which transforms Eq. (24) into

$$\mathbf{I} \mathbf{u}_{m,ii} - \frac{1}{\omega} \mathbf{Q}_m^I \mathbf{u}_{m,i} + (\Omega^2 - \mathbf{Q}_m^R) \mathbf{u}_m = \mathbf{0} \quad (35)$$

In summary, starting from Eqs. (23) and (24), which are based on the linearized CFD technology outlined in Sec. III.A.2, Eq. (35) is derived. Then, the flutter analysis of a given aeroelastic system can be performed in the frequency domain simply by applying the $p - k$ method [26,27] to this equation.

5. Incorporation of the Internal Fluid Models

Equation (23) governs the external flow and therefore is valid independently from the presence or absence of an internal fluid in the structure. However, if the structure contains an internal fluid, Eq. (24) can be modified as follows. First, the added-mass matrix \mathbf{M}_A [Eq. (12)] or its counterpart obtained with mass and inertia lumping can be assembled into the structural mass matrix \mathbf{M}_S . Then, the first n_m natural modes of the structure containing the internal fluid, that is the structure characterized by the finite-element matrices $(\mathbf{M}_S + \mathbf{M}_A)$ and \mathbf{K} , are computed, and Eq. (19) is projected onto the modal basis defined by these modes to obtain a governing equation similar to Eq. (24).

6. Implementation in AERO

Both time domain and frequency domain aspects of the linearized CFD-based computational framework for flutter analysis described previously are implemented in the CFD-based aeroelastic software platform AERO [28,29]. This software has been validated for several wind-tunnel and flight-test configurations, including the AGARD Wing 445.6 and the F-16 Block 40 aircraft [28,29]. Its time-domain capability is used in this work to perform all reported flutter analyses.

7. Implementation in REELC

The frequency domain component of the linearized CFD-based computational framework for flutter analysis described previously is also implemented in the code REELC [30]. Hence, this code is also used in this work to perform and verify all reported flutter analyses.

B. Non-Computational-Fluid-Dynamics-Based Computational Framework

For both purposes of verification and compare-and-contrast, the doublet-lattice method (DLM) and ZONA51 lifting-surface theory are also considered in this work for predicting the sloshing effects of an internal fluid on the flutter envelope of an aeroelastic system. These two methods, which operate in the frequency domain, are complementary representatives of non-CFD-based computational frameworks. They are equipped here with the $p - k$ method for flutter analysis [26,27]. The DLM is commonly used in the aircraft industry for load computations in the subsonic regime, and the ZONA51 lifting-surface theory is typically used for similar computations in supersonic air streams. Both methods can account for interference

among multiple lifting surfaces and bodies. However, ZONA51 assumes planar lifting surfaces. Because both methods are well covered in the literature [19,31,32], they are not overviewed next. Instead, only the ability or inability of these methods to handle aeroelastic configurations with stores and fuel tanks is briefly discussed.

1. Doublet-Lattice Method for Subsonic Flows

To represent the lifting characteristics of bodies like a fuselage, nacelle, or an external store, the slender-body theory has been associated with the DLM [33] in the subsonic domain. The primary wing-body interference is approximated by a system of images of the DLM trailing vortices and doublets within a cylindrical interference body that circumscribes each slender body. The secondary wing-body interference that results from the DLM-bound vortices and doublets is accounted for by a line of doublets located on the longitudinal axis of each slender body. The boundary conditions of no flow through the lifting surfaces or through the body (on the average about the periphery) lead to the equations for the lifting pressure on the surfaces and longitudinal (and/or lateral) loading on the bodies in terms of the normal washes on the wing-body combination.

2. ZONA51 Lifting-Surface Theory for Supersonic Flows

Unlike the DLM, ZONA51 has no extension to slender bodies. Consequently, it cannot handle configurations with stores and fuel tanks. For this reason, it is used in this work primarily for the purpose of verification when assessing the validity of ignoring the store aerodynamics during the flutter analysis of a wing-store configuration with an internal fluid.

3. Implementation in NASTRAN and Incorporation of the Internal Fluid Models

The DLM and ZONA51 packages used in this work are those implemented in the SOL145 “Dynamic Flutter Analysis” of the commercial MSC NASTRAN software. For the purpose of this study, the hydroelastic and frozen-mass models described in Secs. II.A and II.B, respectively, were incorporated in both methods by using NASTRAN’s programming language DMAP (from “Direct Matrix Abstraction Program”) to superpose the added-mass matrix of the internal fluid to the structural mass matrix. Alternatively, the standard virtual mass approach available in NASTRAN could have been used for the same purpose. It was recently verified (see [34]) that both aforementioned approaches give the same results. For both DLM and ZONA51, MSC NASTRAN’s implementation of the $p - k$ method is used for flutter analysis.

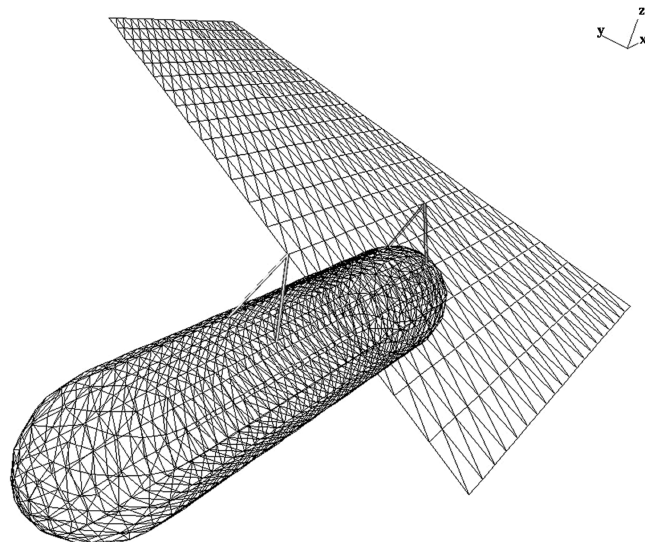


Fig. 2 Wing-store system: hypothetical assembly of the 2.5 ft weakened model 3 of the AGARD Wing 445.6 and a store.

Table 1 Variations with the store fill level of the natural frequencies computed by AERO

Mode	Frequency, Hz ^a								
	0% fill	30.9% fill		50.0% fill		69.1% fill		99.9% fill	
<i>Hydroelastic representation of the internal fluid</i>									
First flexion	11.55	11.42	(-1.10)	11.29	(-2.22)	11.17	(-3.29)	11.05	(-4.32)
Second flexion	39.61	35.52	(-10.34)	33.58	(-15.22)	31.20	(-21.22)	29.50	(-25.52)
First torsion	45.96	37.93	(-17.46)	31.50	(-31.45)	28.19	(-38.67)	25.71	(-44.06)
Second torsion	57.79	53.61	(-7.23)	52.48	(-9.18)	51.96	(-10.09)	51.66	(-10.60)
Third flexion	97.87	93.00	(-4.97)	90.39	(-7.64)	88.77	(-9.30)	85.92	(-12.21)
Third torsion	129.19	126.36	(-2.19)	123.70	(-4.25)	125.89	(-2.55)	125.48	(-2.87)
Store axirotation	158.29	146.70	(-7.32)	129.32	(-18.30)	108.94	(-31.18)	91.78	(-42.02)
Coplanar	163.08	162.40	(-0.42)	161.37	(-1.05)	159.42	(-2.24)	152.40	(-6.55)
<i>Frozen-mass representation of the internal fluid</i>									
First flexion	11.55	11.39	(-1.32)	11.24	(-2.65)	11.09	(-3.93)	10.97	(-5.01)
Second flexion	39.61	35.41	(-10.60)	32.27	(-18.54)	29.93	(-24.45)	28.22	(-28.75)
First torsion	45.96	36.56	(-20.44)	31.00	(-32.54)	27.49	(-40.19)	25.09	(-45.40)
Second torsion	57.79	53.63	(-7.19)	52.53	(-9.10)	52.02	(-9.99)	51.74	(-10.46)
Third flexion	97.87	91.84	(-6.15)	92.33	(-5.66)	83.92	(-14.25)	85.87	(-12.25)
Third torsion	129.19	102.89	(-20.36)	126.29	(-2.24)	125.96	(-2.50)	125.86	(-2.58)
Store axirotation	158.29	127.18	(-19.65)	86.67	(-45.25)	90.28	(-42.96)	91.79	(-42.01)
Coplanar	163.08	159.44	(-2.23)	155.34	(-4.75)	150.92	(-7.45)	147.27	(-9.69)

^aBetween parentheses: percent change with respect to the 0% store fill level.

Table 2 Relative differences between the frequencies computed by AERO using the hydroelastic and frozen-mass models

Discrepancies in the frequencies computed using two different internal fluid models (as a percentage of the frequency computed using the hydroelastic added-mass model)					
Mode	0% fill	30.9% fill	50.0% fill	69.1% fill	99.9% fill
First flexion	—	-0.23	-0.44	-0.66	-0.72
Second flexion	—	-0.30	-3.91	-4.09	-4.34
First torsion	—	-3.61	-1.58	-2.47	-2.40
Second torsion	—	0.05	0.09	0.11	0.15
Third flexion	—	-1.24	2.15	-5.46	-0.05
Third torsion	—	-18.57	2.09	0.06	0.30
Store axirotation	—	-13.31	-32.98	-17.13	0.01
Coplanar	—	-1.82	-3.74	-5.33	-3.37

IV. Flutter Analysis of a Wing–Store Configuration at Different Fill Levels

To develop an insight into the effect of fuel sloshing on the flutter envelope of an aircraft, the flutter analysis of a hypothetical

wing–store configuration filled with JP-8 is considered in this section. The numerical results obtained for different flight regimes and various store fill levels are reported and discussed.

A. Wing–Store Test System

The hypothetical aeroelastic system considered herein consists of the assembly of the 2.5 ft weakened model 3 of the AGARD Wing 445.6 [35] and a store with a 3/32-in.-thick aluminum ($E = 1.44 \times 10^{10}$ lb/ft², $\nu = 0.33$, $\rho_S = 5.24$ slugs/ft³) shell. The internal fluid has the same density as that of JP-8 fuel ($\rho_F = 1.5579$ slugs/ft³). The wing and the store are connected by two sets of linear multipoint constraints (see the Appendix for a detailed description of the geometry).

An undamped finite-element model of the wing with 800 triangular composite shell elements and 2646 DOF is constructed using the information given by Yates [35]. It predicts natural mode shapes and frequencies that are similar to those derived experimentally. The hypothetical store is discretized into 1408 triangular shell elements and 4188 DOF. Figure 2 shows the finite-element mesh of the geometry.

Table 3 Variations with the store fill level of the natural frequencies computed by NASTRAN

Mode	Frequency, Hz ^a								
	0% fill	30.9% fill		50.0% fill		69.1% fill		99.9% fill	
<i>Hydroelastic representation of the internal fluid</i>									
First flexion	11.20	11.00	(-1.79)	10.90	(-2.68)	10.65	(-4.91)	10.60	(-5.36)
Second flexion	39.70	34.53	(-13.02)	32.50	(-18.14)	28.79	(-27.48)	27.80	(-29.97)
First torsion	42.80	35.54	(-16.96)	32.00	(-25.23)	26.65	(-37.73)	25.50	(-40.42)
Second torsion	57.10	49.82	(-12.75)	49.10	(-14.01)	47.98	(-15.97)	48.20	(-15.59)
Third flexion	99.60	92.23	(-7.40)	91.70	(-7.93)	87.87	(-11.78)	87.20	(-12.45)
Third torsion	122.00	117.20	(-3.93)	118.00	(-3.28)	117.00	(-4.10)	119.80	(-1.80)
Store axirotation	162.00	146.60	(-9.51)	130.00	(-19.75)	104.20	(-35.68)	93.00	(-42.59)
Coplanar	176.00	179.90	(2.22)	174.00	(-1.14)	170.00	(-3.41)	155.60	(-11.59)
<i>Frozen-mass representation of the internal fluid</i>									
First flexion	11.20	11.03	(-1.52)	10.80	(-3.57)	10.69	(-4.55)	10.50	(-6.25)
Second flexion	39.70	34.81	(-12.32)	30.60	(-22.92)	29.53	(-25.62)	27.70	(-30.23)
First torsion	42.80	36.31	(-15.16)	32.10	(-25.00)	27.47	(-35.82)	25.30	(-40.89)
Second torsion	57.10	50.60	(-11.38)	49.10	(-14.01)	48.57	(-14.94)	48.30	(-15.41)
Third flexion	99.60	93.38	(-6.24)	93.70	(-5.92)	85.68	(-13.98)	87.40	(-12.25)
Third torsion	122.00	104.90	(-14.02)	119.40	(-2.13)	119.10	(-2.38)	119.00	(-2.46)
Store axirotation	162.00	120.20	(-25.80)	88.40	(-45.43)	91.53	(-43.50)	93.40	(-42.35)
Coplanar	176.00	171.20	(-2.73)	165.40	(-6.02)	159.30	(-9.49)	154.50	(-12.22)

^aBetween parentheses: percent change with respect to the 0% store fill level.

Table 4 Relative differences between the frequencies (ordered according to corresponding mode shapes) computed by NASTRAN using the hydroelastic and frozen-mass models

Mode	Discrepancies in the frequencies computed using different internal fluid models (as a percentage of the frequency computed using the hydroelastic added-mass model)				
	0% fill	30.9% fill	50.0% fill	69.1% fill	99.9% fill
First flexion	—	0.27	-0.92	0.38	-0.94
Second flexion	—	0.81	-5.85	2.57	-0.36
First torsion	—	2.17	0.31	3.08	-0.78
Second torsion	—	1.57	0.00	1.23	0.21
Third flexion	—	1.25	2.18	-2.49	0.23
Third torsion	—	-10.49	1.19	1.79	-0.67
Store axirotation	—	-18.01	-32.00	-12.16	0.43
Coplanar	—	-4.84	-4.94	-6.29	-0.71

B. Simulated Ground Vibrations

Because in both computational frameworks adopted in this work the structure is represented by its natural modes, an eigenanalysis of the aeroelastic system described previously is first performed for various store fill levels. In general, the results obtained using AERO and NASTRAN are in good agreement, with relative discrepancies lower than 7% for all frequencies. For this reason, the analysis reported next refers only to the AERO computational results (see Tables 1 and 2). However, the NASTRAN counterparts are also provided for reference (see Tables 3 and 4).

Table 1 reports the first natural frequencies computed by AERO and listed using their physical description. The reader can observe that these two models of the internal fluid lead to a general trend of decreasing frequencies with increasing store fill levels. However, both models lead to results that also differ in an interesting manner. When the hydroelastic model of the internal fluid is used, the computed frequencies decrease monotonically with an increasing fill level. However, when the frozen-mass model is used, some frequencies, namely those associated with the third flexional and torsional modes, reach their minima at intermediate fill levels. Moreover, one can see that the store fill level affects some modes more significantly than others. As this fill level increases from 0 to 99%, the natural frequencies corresponding to the second bending

mode and store-roll modes drop by more than 40%, whereas those corresponding to the other modes drop by as little as 3%.

Table 2 reports the relative discrepancies between those eigenfrequencies computed using the hydroelastic and frozen-mass models. Except for certain frequencies that are identically computed (within 0.5% discrepancy) using either model, the frozen-mass model tends to lead to lower frequencies than the hydroelastic model for the same fill level. The largest discrepancies are observed at intermediate fill levels (e.g., 30.9, 50, and 69.1%). In any case, the reader can observe that freezing the mass of the internal fluid instead of accounting for its small motion relative to the containing structure leads to the overestimation of the added-mass effect. Moreover, the hydroelastic model essentially predicts a monotonic decrease in the frequency for the first three torsional/bending modes, the coplanar mode, and the store-roll mode (which, as its name suggests, is predominantly characterized by the displacement of the store). This suggests that the effect of the internal fluid increases when the store fill level is increased. However, the frozen-mass model predicts that the presence of the internal fluid alters most significantly the frequency of the store-roll mode at the 50% fill level. It is furthermore observed that the largest differences between the frequencies obtained using the two internal fluid models occur for the store-roll mode. This is expected because the representation of the roll inertia of the fluid differs significantly from one model to the other.

C. Flutter Analysis

Next, the results of the flutter analysis performed on the wing-store test configuration using both computational frameworks described previously are reported and discussed. In both cases, the structure is represented by its first 10 natural modes. Flutter predictions are performed for various freestream Mach numbers spanning the subsonic, transonic, and early supersonic flow regimes, following the guidelines established by Yates [35] for the stand-alone AGARD Wing 445.6 configuration (see Table 5).

1. AERO Results

First, the CFD-based results obtained using the higher-fidelity code AERO are presented. Table 6 reports, for both internal fluid models considered in this work and various freestream Mach numbers M_∞ , the variation with the store fill level of the critical

Table 5 Freestream parameters chosen for the flutter analysis [35]

M_∞	0.499	0.678	0.901	0.960	1.072	1.141	1.201	1.272
ρ_∞ , kg/m ³	0.4278	0.2082	0.0995	0.0634	0.0551	0.0783	0.0644	0.0593
ρ_∞ , slugs/ft ³	0.000830	0.000404	0.000193	0.000123	0.000107	0.000152	0.000125	0.000115

Table 6 Variations of the critical freestream velocity with the store fill level predicted by AERO

M_∞	Fuel model	V_{∞}^{cr} , ft/s ^a										
		0% fill	15.0% fill	30.9% fill	50.0% fill	69.1% fill	99.9% fill					
0.499	Hydroelastic	695.6	721.4 (3.71)	708.0 (1.78)	682.1 (-1.95)	652.4 (-6.21)	627.0 (-9.86)					
0.499	Frozen mass	695.6	720.0 (3.52)	703.7 (1.17)	668.3 (-3.92)	631.4 (-9.23)	593.2 (-14.72)					
0.678	Hydroelastic	981.5	995.1 (1.38)	978.8 (-0.28)	956.1 (-2.59)	928.7 (-5.38)	902.6 (-8.04)					
0.678	Frozen mass	981.5	993.4 (1.20)	975.7 (-0.60)	944.0 (-3.82)	907.9 (-7.50)	872.5 (-11.11)					
0.901	Hydroelastic	1260.9	1256.4 (-0.36)	1241.7 (-1.52)	1222.5 (-3.05)	1200.6 (-4.78)	1182.9 (-6.19)					
0.901	Frozen mass	1260.9	1254.8 (-0.49)	1236.0 (-1.98)	1212.9 (-3.81)	1183.5 (-6.14)	1162.4 (-7.82)					
0.960	Hydroelastic	1279.2	1266.9 (-0.97)	1251.9 (-2.14)	1223.9 (-4.32)	1190.0 (-6.97)	1171.3 (-8.43)					
0.960	Frozen mass	1279.2	1235.2 (-3.44)	1193.7 (-6.68)	1187.4 (-9.91)	1163.3 (-9.06)	1128.7 (-11.77)					
1.072	Hydroelastic	2199.8	2172.2 (-1.26)	2107.7 (-4.19)	1997.8 (-9.18)	1917.1 (-12.85)	1857.4 (-15.57)					
1.072	Frozen mass	2199.8	2158.4 (-1.88)	2064.4 (-6.16)	1916.2 (-12.89)	1783.0 (-18.95)	1689.5 (-23.20)					
1.141	Hydroelastic	1419.3	1393.8 (-1.80)	2218.4 (56.30)	1983.8 (39.77)	1819.2 (28.17)	1709.1 (20.42)					
1.141	Frozen mass	1419.3	1378.2 (-2.90)	2139.8 (50.76)	1863.0 (31.26)	1701.5 (19.88)	1600.4 (12.76)					
1.201	Hydroelastic	1139.7	1122.5 (-1.50)	2500.4 (119.40)	2168.2 (90.25)	1919.2 (68.40)	1761.2 (54.53)					
1.201	Frozen mass	1139.7	1143.9 (0.37)	2358.8 (106.97)	1868.0 (63.91)	1712.1 (50.22)	1617.7 (41.95)					
1.272	Hydroelastic	3141.4	3026.4 (-3.66)	2847.3 (-9.36)	2589.5 (-17.57)	2408.9 (-23.32)	2285.5 (-27.24)					
1.272	Frozen mass	3141.4	3029.1 (-3.57)	2735.1 (-12.93)	2436.7 (-22.45)	2207.7 (-29.72)	2069.5 (-34.12)					

^aBetween parentheses: percent change with respect to 0% store fill level.

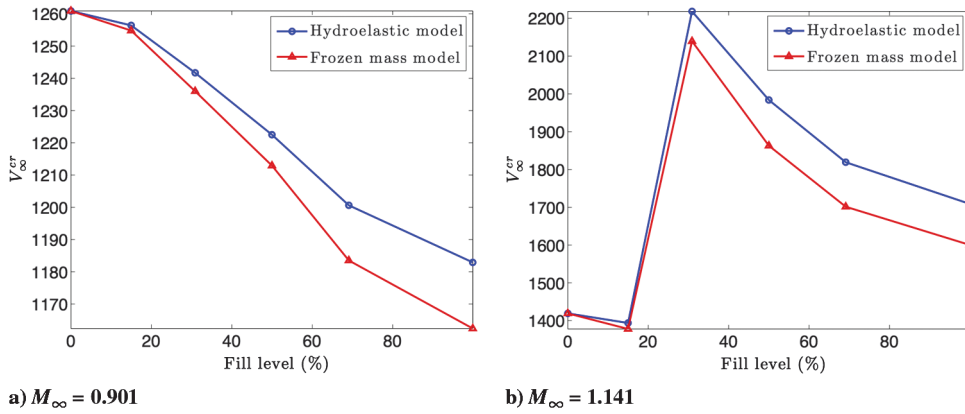


Fig. 3 Variations of the critical freestream velocity with the store fill level predicted by AERO.

values V_{∞}^{cr} of the freestream velocity, that is its values at the onset of flutter.

Regardless of the internal fluid model used, the critical flutter speed, and therefore also the critical pressure, predicted by AERO are found to generally decrease with an increasing fill level, meaning that flutter onsets earlier at higher fill levels. Also, these critical quantities are found to change most significantly as the fill level varies from 30 to 70%. Exceptions are noticeable, however, at the two supersonic Mach numbers $M_{\infty} = 1.141$ (see Fig. 3) and $M_{\infty} = 1.201$, where AERO predicts that the aforementioned critical quantities significantly increase when the fill level is increased from less than 20 to about 31%, before they decrease when the fill level is further increased.

Overall, the reader can observe that the choice between the two internal fluid models considered in this work has little impact on the critical quantities predicted by AERO. In most cases, the difference between the critical velocity values, and therefore critical pressure values, computed using both models are within a few percent of the corresponding zero-fill reference values (see Fig. 3). Nevertheless, large relative differences are found for the case $M_{\infty} = 1.201$, where the reference critical quantities are very small.

To characterize further the dependence on the flight conditions of the impact of the internal fluid model, the following quantity:

$$f(V_{\infty}^{cr}) = \frac{V_{\infty, \text{frozen}}^{cr} - V_{\infty, \text{hydroelastic}}^{cr}}{V_{\infty, \text{hydroelastic}}^{cr}}$$

is plotted in Fig. 4. At all Mach numbers where the critical speed decreases monotonically with the increasing fill level, two observations are noteworthy. First, f is almost always negative, meaning that the frozen-mass representation of the internal fluid

underpredicts the flutter quantities or, in other words, overestimates the added-mass effects of the internal fluid, in comparison to the hydroelastic representation of the internal fluid. Second, in most cases, the absolute value of f increases with the store fill level. Therefore, the overprediction of the added-mass effects is exacerbated by an increasing fill level. At Mach 1.201 and fill level 15%, f becomes positive. This means that, at these conditions, the cruder frozen-mass model overpredicts the size of the flight envelope. Given that this model is an approximation of the hydroelastic model, the following comment can be reasonably added. From a design perspective, these findings imply that the frozen-mass model could be treacherous because, if relied on, it could lead to a design configuration that may experience unexpected flutter at certain flight conditions.

Next, Fig. 5 reports the computed variations of the flutter speed index with the freestream Mach number for the half-full store and almost-full store cases, and both internal fluid models. Here, the flutter speed index is defined as

$$FSI = \left(\frac{V_{\infty}^{cr}}{b_s \omega_{\alpha} \sqrt{\bar{\mu}}} \right) \quad (36)$$

where ω_{α} is the first dry torsional mode of the structural system; b_s is the semichord of the wing at the root; and $\bar{\mu} = (m_s / \rho_{\infty} \hat{V})$, where ρ_{∞} is the freestream density of the test medium. In the absence of a store, \hat{V} is the volume of a conical frustum with lower and upper base diameters equal to the streamwise root and tip chords of the wing, respectively, and height equal to the wing semispan; and m_s is the structural mass of the wing [35]. In the context of this work, the volume of the smallest cylinder enclosing the store is added to \hat{V} , and the structural mass of the empty store is added to m_s . The reader can observe that, at certain flight conditions (e.g., $M_{\infty} = 0.96$ and

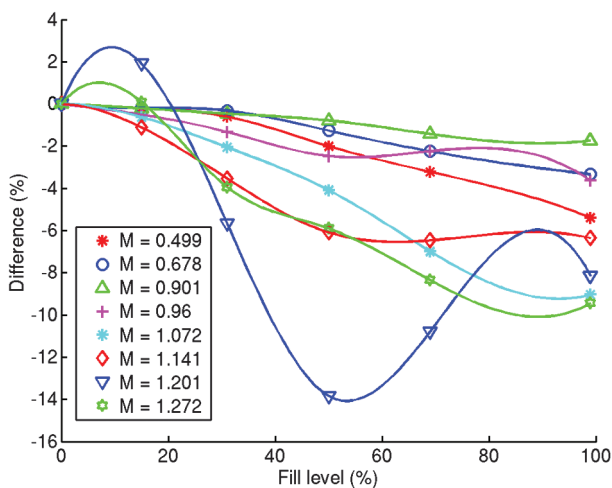


Fig. 4 Variations with the store fill level of the relative difference in the critical speeds computed by AERO due to the difference between the two considered internal fluid models.

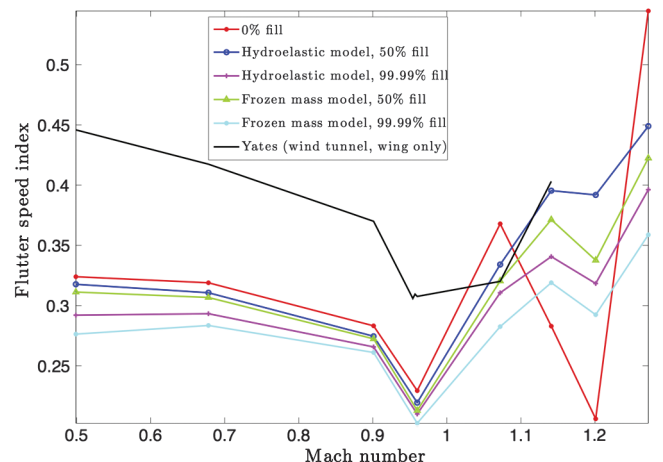


Fig. 5 Variations of the flutter speed index with the freestream Mach number predicted by AERO.

Table 7 Variations of the critical freestream velocity with the store fill level predicted by REELC in supersonic domain

M_∞	Fuel model	V_{∞}^{cr} , ft/s ^a										
		0% fill		15.0% fill		30.9% fill		50.0% fill		69.1% fill		99.9% fill
1.072	Hydroelastic	2205.8	2168.9	(-1.7)	2021.3	(-8.4)	1917.9	(-13.1)	1792.6	(-18.7)	1725.2	(-21.8)
1.072	Frozen mass	2205.8	2148.0	(-2.6)	2003.9	(-9.2)	1792.9	(-18.7)	1628.5	(-26.2)	1514.9	(-31.3)
1.141	Hydroelastic	1447.3	1389.0	(-4.0)	2017.8	(39.4)	1805.9	(24.7)	1645.8	(13.7)	1500.1	(3.6)
1.141	Frozen mass	1447.3	1337.2	(-7.6)	1952.1	(34.9)	1718.0	(18.7)	1594.4	(10.1)	1514.4	(4.6)
1.201	Hydroelastic	1861.3	1723.2	(-7.4)	2450.5	(31.6)	2198.7	(18.1)	2004.6	(7.7)	1918.7	(3.1)
1.201	Frozen mass	1861.3	1614.9	(-13.2)	2373.6	(27.5)	2013.4	(8.2)	1832.3	(-1.6)	1728.5	(-7.1)
1.272	Hydroelastic	3277.2	3139.0	(-4.2)	2700.2	(-17.6)	2477.2	(-24.4)	2269.7	(-30.7)	2188.3	(-33.2)
1.272	Frozen mass	3277.2	3081.0	(-6.0)	2672.2	(-18.5)	2269.8	(-30.7)	2038.3	(-37.8)	1906.9	(-41.8)

^aBetween parentheses: percent change with respect to 0% store fill level.

$M_\infty = 1.072$), the flutter speed index is affected by the choice of the internal fluid model as much as, if not more than, taking into account the presence of an internal fluid in the flutter analysis.

2. REELC Results

Next, the computational results obtained for supersonic airstreams using the higher-fidelity code REELC are presented in Table 7. These results are in good agreement with those predicted by the code AERO (see Fig. 6).

3. NASTRAN Results

Finally, the flutter analysis results obtained using NASTRAN are summarized in Table 8. For subsonic airstreams, the comparison

of the critical freestream velocities obtained using the DLM and AERO is performed in Fig. 7. The reader can observe that AERO and NASTRAN predict similar results that lead to the same conclusions.

In supersonic airstreams, the comparison of the results obtained using NASTRAN (ZONA51), AERO, and REELC is performed in Fig. 6. Here, the reader can observe that the lower-fidelity ZONA51 method cannot reproduce the results of the higher-fidelity CFD-based codes AERO and REELC. The discrepancies are due primarily to the absence of the aerodynamics of the tank from the ZONA51 computational model due itself to the inability of this method to deal with slender bodies. (This explanation was verified by repeating the flutter analysis in supersonic airstreams for the computational

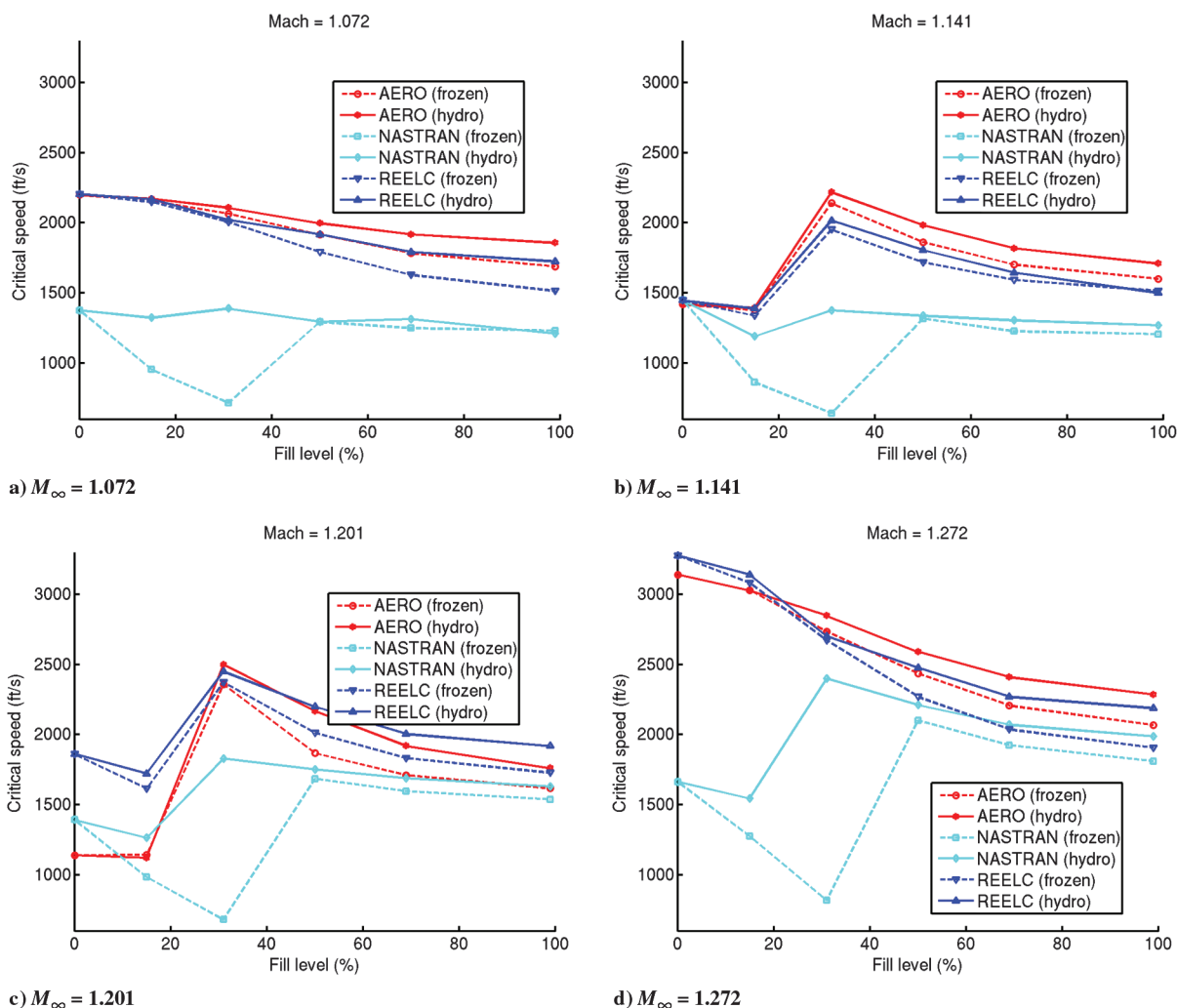


Fig. 6 Comparison of the variations of the critical freestream velocity with the store fill level predicted by AERO, REELC, and NASTRAN (ZONA51) for supersonic airstreams.

Table 8 Variations of the critical freestream velocity with the store fill level predicted by NASTRAN

M_∞	Fuel model	V_∞^{cr} , ft/s ^a										
		0% fill	15.0% fill	30.9% fill	50.0% fill	69.1% fill	99.9% fill					
0.499	Hydroelastic	669.1	666.0	(-0.5)	652.3	(-2.5)	628.9	(-6.0)	606.6	(-9.3)	584.7	(-12.6)
0.499	Frozen mass	669.1	664.3	(-0.7)	647.6	(-3.2)	616.5	(-7.9)	583.8	(-12.7)	558.2	(-16.6)
0.678	Hydroelastic	919.8	916.0	(-0.4)	903.8	(-1.7)	881.3	(-4.2)	860.9	(-6.4)	838.6	(-8.8)
0.678	Frozen mass	919.8	913.9	(-0.6)	897.9	(-2.4)	871.3	(-5.3)	840.2	(-8.7)	809.9	(-11.9)
0.901	Hydroelastic	1156.2	1154.0	(-0.2)	1141.4	(-1.3)	1120.5	(-3.1)	1105.3	(-4.4)	1089.7	(-5.7)
0.901	Frozen mass	1156.2	1151.0	(-0.4)	1135.9	(-1.8)	1114.0	(-3.6)	1091.3	(-5.6)	1071.4	(-7.3)
0.960	Hydroelastic	1275.6	1272.0	(-0.3)	1259.2	(-1.3)	1234.0	(-3.3)	1221.1	(-4.3)	1204.6	(-5.6)
0.960	Frozen mass	1275.6	1268.9	(-0.5)	1252.5	(-1.8)	1228.6	(-3.7)	1206.8	(-5.4)	1186.8	(-7.0)
1.072	Hydroelastic	1376.5	1323.4	(-3.9)	1389.3	(0.9)	1294.5	(-6.0)	1313.4	(-4.6)	1209.9	(-12.1)
1.072	Frozen mass	1376.5	954.3	(-30.7)	717.1	(-47.9)	1294.1	(-6.0)	1249.8	(-9.2)	1232.5	(-10.5)
1.141	Hydroelastic	1447.3	1189.5	(-17.8)	1376.3	(-4.9)	1337.2	(-7.6)	1303.7	(-9.9)	1269.4	(-12.3)
1.141	Frozen mass	1447.3	862.3	(-40.4)	642.6	(-55.6)	1318.1	(-8.9)	1226.9	(-15.2)	1206.2	(-16.7)
1.201	Hydroelastic	1392.4	1264.4	(-9.2)	1829.0	(31.3)	1752.6	(25.9)	1689.0	(21.3)	1631.2	(17.1)
1.201	Frozen mass	1392.4	984.4	(-29.3)	681.9	(-51.0)	1685.3	(21.0)	1597.1	(14.7)	1537.8	(10.4)
1.272	Hydroelastic	1664.4	1544.5	(-7.2)	2399.5	(44.1)	2210.0	(32.8)	2070.1	(24.4)	1988.1	(19.4)
1.272	frozEn mass	1664.4	1274.7	(-23.4)	818.7	(-50.8)	2100.2	(26.2)	1924.3	(15.6)	1810.8	(8.8)

^aBetween parentheses: percent change with respect to 0% store fill level.

aeroelastic model excluding the aerodynamics of the tank using AERO and REELC, and reproducing the results obtained using ZONA51.) On the other hand, the reader can observe once again that AERO and REELC deliver relatively close predictions. This suggests that the aerodynamics of a store cannot be, in general, ignored when performing the aeroelastic analysis of a wing-store configuration.

4. Further Discussion of the Impact of the Chosen Model for the Internal Fluid

Figure 8 highlights the differences found between the critical freestream velocities predicted using a hydroelastic model for the internal fluid or a frozen-mass simplification and the various software packages considered in this work. These differences tend to be

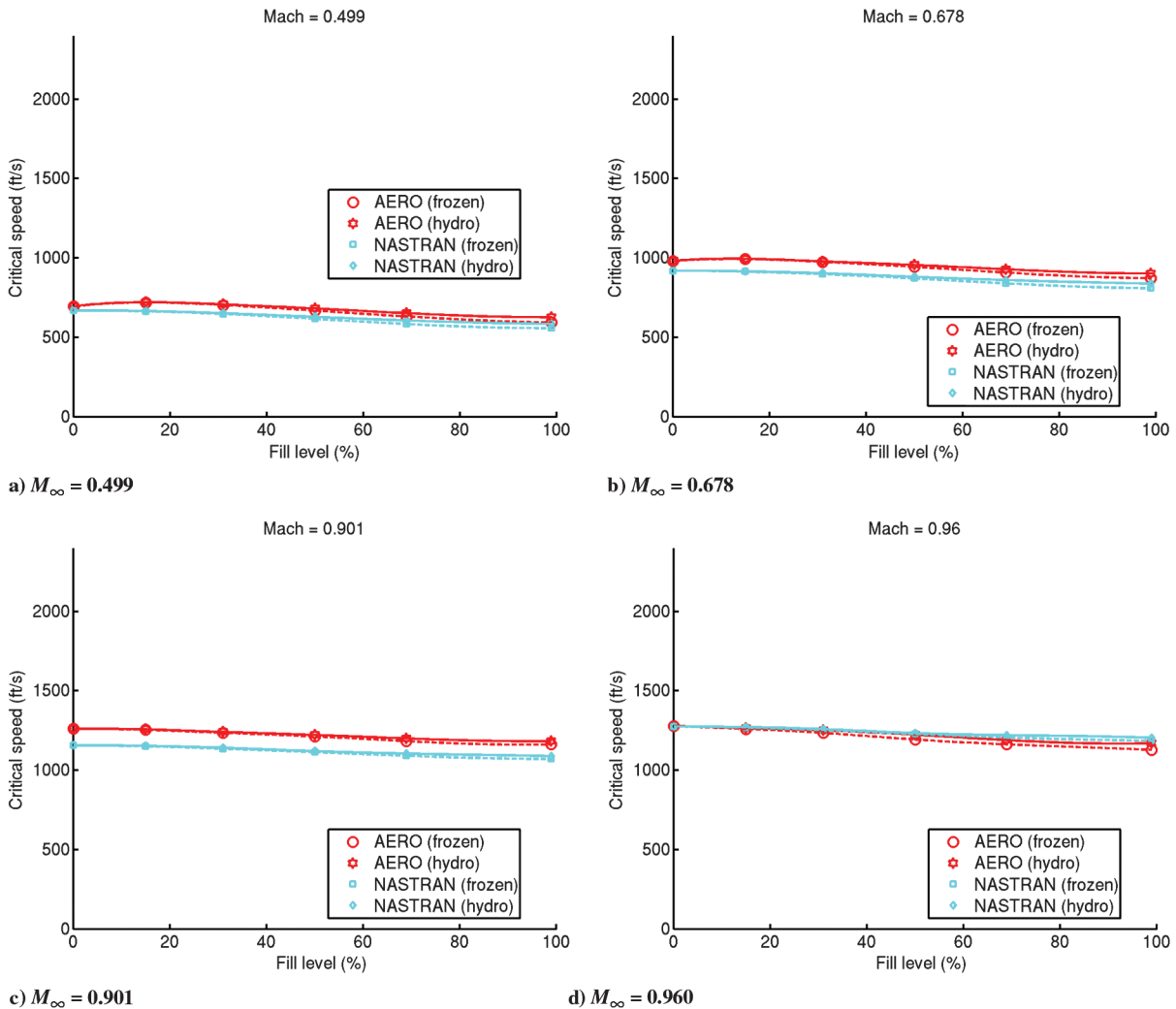


Fig. 7 Comparison of the variations of the critical freestream velocity with the store fill level predicted by AERO and NASTRAN (DLM) for subsonic airstreams.

smaller in the subsonic regime (below 6%) and larger in supersonic airstreams (above 10%). Interestingly, however, except for the case of the fill level of 99% at $M_\infty = 1.141$, these differences have always the same negative sign, at least for the wing-store configuration

considered in this work. This suggests that the frozen-mass assumption is most often a conservative one, in the sense that it leads to smaller critical freestream velocities than the hydroelastic model for the internal fluid.

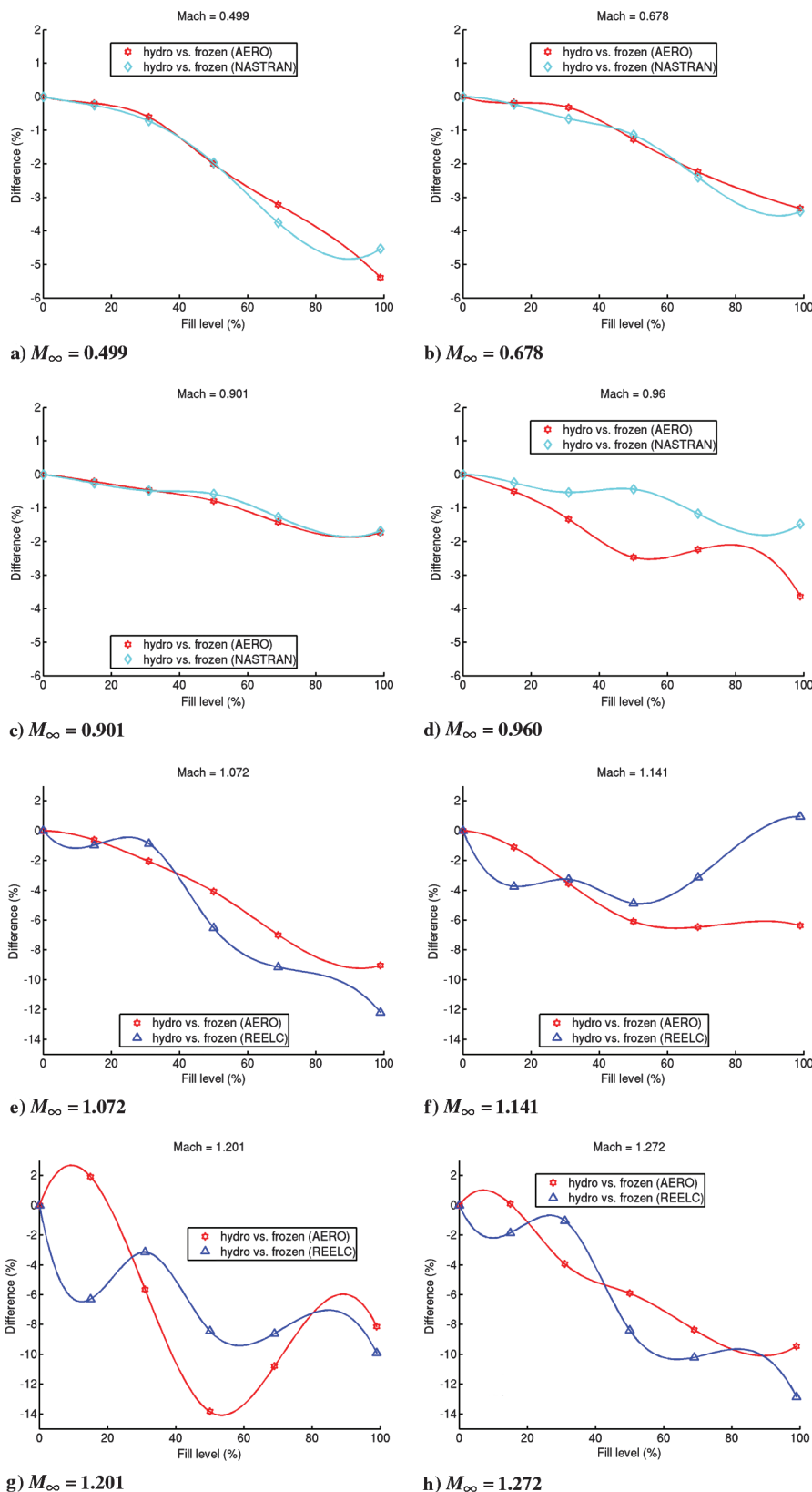


Fig. 8 Differences between the critical freestream velocities predicted using a hydroelastic model of the internal fluid or a frozen-mass simplification and AERO, REELC, and NASTRAN.

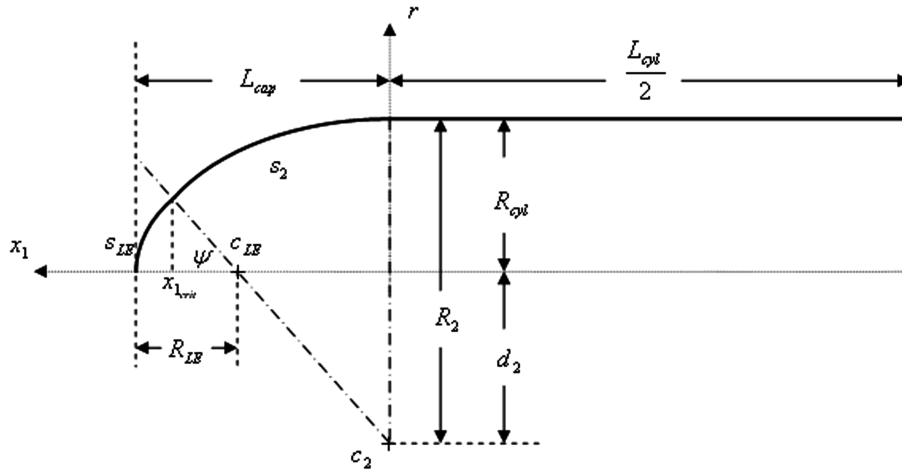


Fig. A1 Axisymmetric quarter cross section of the store.

V. Conclusions

Flutter computations were performed for a wing–store test configuration in subsonic, transonic, and early supersonic air streams, using both computational-fluid-dynamics-based and linear-theory-based computational frameworks. Various JP-8 fill levels of the store were considered. In each case, the fuel was represented using both a hydroelastic added-mass model, which accounts for the sloshing effect, and a frozen-mass model, which ignores it. Both independent sets of obtained computational results suggest that, in general, the critical pressure and flutter speed decrease with an increasing fill level. They also reveal that ignoring the hydroelastic vibration effect by representing the internal fluid as a simplified frozen mass leads to natural frequencies of the dry wing–store system that are more sensitive than otherwise to the store fill level. More importantly, they also suggest that, in general, but not necessarily at all speeds, ignoring the hydroelastic effect tends to overestimate the added-mass effect and underestimate the critical pressure and flutter speed. The obtained sets of computational results also reveal that, at least in the supersonic regime, excluding the aerodynamics of the store from the computational aeroelastic model, for example to accelerate parameteric studies, leads to erroneous numerical predictions.

Acknowledgments

The Stanford University authors acknowledge partial support by a research grant from the King Abdulaziz City for Science and Technology, partial support by The Boeing Company under Contract Sponsor Ref 45047, and partial support by the U.S. Air Force Office of Scientific Research under grant FA9550-10-1-0539. Any opinions, findings, conclusions, or recommendations expressed in this document are those of the authors and do not necessarily reflect the views of the sponsors.

Appendix A: Store Geometry

The test geometry considered in Sec. IV.A consists of the 2.5 ft weakened model 3 of the AGARD Wing 445.6 [35] and an axisymmetric store with smooth front and back ends. Using a coordinate system (in feet) centered at the leading edge of the root of the wing (the same system as in Yates [35]), the store is positioned so that its front tip is in the plane $x = -0.1667$ and its centerline is at the intersection of the planes $y = 0.75$ and $z = -0.375$. The wing and the store are connected by two sets of linear multipoint constraints. The first set connects the point on the wing with coordinates (0.7966, 0.7500, 0.0000) to the two points on the store with coordinates (0.7395, 0.6783, -0.2018) and (0.7395, 0.8218, -0.2018), respectively. The second set connects the point (1.947, 0.7500, 0.0000) on the wing to the two points (2.000, 0.6783, -0.2018) and (2.000, 0.8218, -0.2018) on the store (see Fig. 2).

The store is a cylinder capped at both ends by identical tapered sections, each of which begins with a spherical tip then varies

smoothly toward the cylindrical section. The following figure shows a quarter of the store cross section through the centerline (the remainder of the store profile can be obtained by symmetry) and highlights the parameters that completely define the geometry.

Each cross section of a tapered section has two arcs: the leading-edge arc s_{LE} , and the arc s_2 , which connects the leading-edge arc to the cylindrical section. These two arcs are centered at c_{LE} and c_2 , respectively. The arc s_2 is tangent to s_{LE} at one end and tangent to the line representing the cross section of the cylindrical wall at the other end.

The values of the parameters shown in Fig. A1 are as follows: $R_{cyl} = 0.1875$ ft, $L_{cyl} = 1.8333$ ft, $L_{cap} = 0.3333$ ft, $R_{LE} = 0.04249$ ft, and $\psi = 47^\circ$. From these values and the tangency conditions stated previously, it follows that $R_2 = 0.4099$ ft and $d_2 = 0.2224$ ft.

The local coordinates are aligned so that the x_1 axis runs along the centerline of the store, from the root to the tip of the tapered section. The variation of the radius of the tapered section with the coordinate x_1 is given by

$$r(x_1) = \begin{cases} \sqrt{R_2^2 - x_1^2} + (R_{cyl} - R_2), & x_1 \leq x_{1crit} \\ R_{LE} \sin\left(\cos^{-1}\left(1 - \frac{L_{cap} - x_1}{R_{LE}}\right)\right), & x_1 > x_{1crit} \end{cases}$$

where $x_{1crit} = L_{cap} - R_{LE}(1 - \sin(90^\circ - \psi))$.

The wall thickness of the store t_{wall} is relatively small. Hence, the mass of the empty store can be computed as follows:

$$m_{store}^{empty} = 2\pi\rho_{aluminum}t_{wall}\left(L_{cyl}R_{cyl} + 2\int_0^{L_{cap}} r(x_1) dx_1\right)$$

References

- [1] Cazier, F. W. Jr., Doggett, R. V., Jr., and Ricketts, R. H., "Structural Dynamic and Aeroelastic Considerations for Hypersonic Vehicles," NASA TM-104110, 1991.
- [2] Runyan, H. L., and Morgan, H. G., "Flutter at Very High Speeds," NASA TN-D-942, 1961.
- [3] Braslow, A. L., "Propellant Slosh Loads," NASA Space Vehicle Design Criteria (Structures), NASA SP-8009, 1968.
- [4] Bauer, H. F., "Theory of Liquid Sloshing in Compartmented Cylindrical Tanks Due to Bending Excitation," *AIAA Journal*, Vol. 1, No. 7, 1963, pp. 1590–1596. doi:10.2514/3.1862
- [5] Dawson, K. S., and Sussingham, J. C., "F-16 Limit Cycle Oscillation Testing with Asymmetric Store," *17th Applied Aerodynamics Conference*, AIAA Paper 1999-3142, 1999.
- [6] Harris, C., "Accelerated Flutter Testing: A Possible Technique to Expedite Flutter Testing for New Aircraft," *USAF Developmental Test and Evaluation Summit*, AIAA Paper 2004-6822, 2004.

- [7] Peterson, L. D., Crawley, E. F., and Hansman, R., "Nonlinear Fluid Slosh Coupled to the Dynamics of a Spacecraft," *AIAA Journal*, Vol. 27, No. 9, 1989, pp. 1230–1240.
doi:10.2514/3.10250
- [8] Ferman, M. A., and Unger, W. H., "Fluid–Structure Interaction Dynamics in Aircraft Fuel Tanks," *Journal of Aircraft*, Vol. 16, No. 12, 1979, pp. 885–890.
doi:10.2514/3.58616
- [9] Amsallem, D., and Farhat, C., "Stabilization of Projection-Based Reduced-Order Models," *International Journal of Numerical Methods in Engineering*, Vol. 91, No. 4, 2012, pp. 358–377.
doi:10.1002/nme.4274
- [10] Firouz-Abadi, R., Zarifian, P., and Haddadpour, H., "Effect of Fuel Sloshing in the External Tank on the Flutter of Subsonic Wings," *Journal of Aerospace Engineering*, 2012.
doi:10.1061/(ASCE)AS.1943-5525.0000261
- [11] Morand, H. J.-P., and Ohayon, R., *Fluid Structure Interactions: Applied Numerical Methods*, Wiley, New York, 1995, pp. 41–70, 95–110, Chaps. 3, 5.
- [12] Schotté, J.-S., and Ohayon, R., "Various Modelling Levels to Represent Internal Liquid Behaviour in the Vibratory Analysis of Complex Structures," *Computer Methods in Applied Mechanics and Engineering*, Vol. 198, Nos. 21–26, 2009, pp. 1913–1925.
doi:10.1016/j.cma.2008.12.016
- [13] Lesoinne, M., Sarkis, M., Hetmaniuk, U., and Farhat, C., "A Linearized Method for the Frequency Analysis of Three-Dimensional Fluid/Structure Interaction Problems in All Flow Regimes," *Computer Methods in Applied Mechanics and Engineering*, Vol. 190, Nos. 24–25, 2001, pp. 3121–3146.
doi:10.1016/S0045-7825(00)00385-6
- [14] Lesoinne, M., and Farhat, C., "A CFD Based Method for Solving Aeroelastic Eigenproblems in the Subsonic, Transonic, and Supersonic Regimes," *Journal of Aircraft*, Vol. 38, No. 4, 2001, pp. 628–635.
doi:10.2514/2.2839
- [15] Lieu, T., Farhat, C., and Lesoinne, M., "Reduced-Order Fluid/Structure Modeling of a Complete Aircraft Configuration," *Computer Methods in Applied Mechanics and Engineering*, Vol. 190, Nos. 41–43, 2006, pp. 5730–5742.
doi:10.1016/j.cma.2005.08.026
- [16] Farhat, C., Lesoinne, M., and Maman, N., "Mixed Explicit/Implicit Time Integration of Coupled Aeroelastic Problems: Three-Field Formulation, Geometric Conservation and Distributed Solution," *International Journal of Numerical Methods in Fluids*, Vol. 21, No. 10, 1995, pp. 807–835.
doi:10.1002/flid.1650211004
- [17] Albano, E., and Rodden, W. P., "A Doublet-Lattice Method for Calculating Lift Distributions on Oscillating Surfaces in Subsonic Flows," *AIAA Journal*, Vol. 7, No. 2, 1969, pp. 279–285.
doi:10.2514/3.55530
- [18] Rodden, W. P., Giesing, J. P., and Kalman, T. P., "Refinement of the Nonplanar Aspects of the Subsonic Doublet-Lattice Lifting Surface Method," *Journal of Aircraft*, Vol. 9, No. 1, 1972, pp. 69–73.
doi:10.2514/3.44322
- [19] Liu, D. D., James, D. K., Chen, P. C., and Pototzky, A. S., "Further Studies of Harmonic Gradient Method for Supersonic Aeroelastic Applications," *Journal of Aircraft*, Vol. 28, No. 9, 1991, pp. 598–605.
doi:10.2514/3.46070
- [20] Lesoinne, M., and Farhat, C., "Stability Analysis of Dynamic Meshes for Transient Aeroelastic Computations," *11th Computational Fluid Dynamics Conference*, AIAA Paper 1993-3325, July 1993.
- [21] Farhat, C., Lesoinne, M., and LeTallec, P., "Load and Motion Transfer Algorithms for Fluid/Structure Interaction Problems with Non-Matching Discrete Interfaces: Momentum and Energy Conservation, Optimal Discretization and Application to Aeroelasticity," *Computational Methods in Applied Mechanics and Engineering*, Vol. 157, Nos. 1–2, 1998, pp. 95–114.
doi:10.1016/S0045-7825(97)00216-8
- [22] Lesoinne, M., and Farhat, C., "A Higher-Order Subiteration Free Staggered Algorithm for Nonlinear Transient Aeroelastic Problems," *AIAA Journal*, Vol. 36, No. 9, 1998, pp. 1754–1756.
doi:10.2514/2.7555
- [23] Farhat, C., and Lesoinne, M., "Two Efficient Staggered Procedures for the Serial and Parallel Solution of Three-Dimensional Nonlinear Transient Aeroelastic Problems," *Computer Methods in Applied Mechanics and Engineering*, Vol. 182, No. 3, 2000, pp. 499–516.
doi:10.1016/S0045-7825(99)00206-6
- [24] Farhat, C., van der Zee, G., and Geuzaine, P., "Provably Second-Order Time-Accurate Loosely-Coupled Solution Algorithms for Transient Nonlinear Computational Aeroelasticity," *Computer Methods in Applied Mechanics and Engineering*, Vol. 195, Nos. 17–18, 2006, pp. 1973–2001.
doi:10.1016/j.cma.2004.11.031
- [25] Juang, J.-N., and Pappa, R. S., "An Eigensystem Realization Algorithm for Modal Parameter Identification and Model Reduction," *Journal of Guidance, Control, and Dynamics*, Vol. 8, No. 5, 1985, pp. 620–627.
doi:10.2514/3.20031
- [26] Frazer, R. A., and Duncan, W. J., "The Flutter of Aeroplane Wings," British A.R.C., Rept. 1155, 1928.
- [27] Hassig, H. J., "An Approximate True Damping Solution of the Flutter Equation by Determinant Iteration," *Journal of Aircraft*, Vol. 8, No. 11, 1971, pp. 885–889.
doi:10.2514/3.44311
- [28] Geuzaine, P., Brown, G., Harris, C., and Farhat, C., "Aeroelastic Dynamic Analysis of a Full F-16 Configuration for Various Flight Conditions," *AIAA Journal*, Vol. 41, No. 3, 2003, pp. 363–371.
doi:10.2514/2.1975
- [29] Farhat, C., Geuzaine, P., and Brown, G., "Application of a Three-Field Nonlinear Fluid–Structure Formulation to the Prediction of the Aeroelastic Parameters of an F-16 Fighter," *Computers and Fluids*, Vol. 32, No. 1, 2003, pp. 3–29.
doi:10.1016/S0045-7930(01)00104-9
- [30] Mortchéléwicz, G., "Aircraft Aeroelasticity Computed with Linearized RANS Equations," *Proceedings of the 43rd Annual Conference on Aerospace Sciences*, Dan Knassim Ltd., Paper 34, 2003.
- [31] Rodden, W., and Johnson, E., *Aeroelastic Analysis — User's Guide*, MSC Software, Santa Ana, CA, 2002, pp. 17–86, Chap. 2.
- [32] Blair, M., "A Compilation of the Mathematics Leading to the Doublet Lattice Method," U.S. Air Force Research Laboratory TR-92-3028, Wright-Patterson AFB, OH, 1992.
- [33] Giesing, J. P., Kalman, T. P., and Rodden, W. P., "Subsonic Steady and Oscillatory Aerodynamics for Multiple Interfering Wings and Bodies," *Journal of Aircraft*, Vol. 9, No. 10, 1972, pp. 693–702.
doi:10.2514/3.59066
- [34] Schotté, J.-S., Miras, T., and Ohayon, R., "Effect of internal liquids on the vibrations of aerospace structures," *53rd AIAA/ASME/ASCE/AHS/ASC Structures, Structural Dynamics and Materials Conference*, AIAA Paper 2012-1887, April 2012.
- [35] Yates, E. C., "AGARD Standard Aeroelastic Configuration for Dynamic Response, Candidate Configuration 1.—Wing 445.6," NASA TM-100492, 1987.

L. Tichy
Associate Editor